JOC The Journal of Organic Chemistry

Article

pubs.acs.org/joc

Lower Rim 1,3-Di{4-antipyrine}amide Conjugate of Calix[4]arene: Synthesis, Characterization, and Selective Recognition of Hg^{2+} and Its Sensitivity toward Pyrimidine Bases

Jayaraman Dessingou,[†] Khatija Tabbasum,[†] Atanu Mitra,[†] Vijaya Kumar Hinge,[‡] and Chebrolu P. Rao*[,†,‡]

[†]Bioinorganic Laboratory, Department of Chemistry and [‡]Department of Biosciences and Bioengineering, Indian Institute of Technology Bombay, Powai, Mumbai 400076, India

Supporting Information

ABSTRACT: The structurally characterized lower rim 1,3-di{4-antipyrine}amide conjugate of calix[4]arene (**L**) exhibits high selectivity toward Hg^{2+} among other biologically important metal ions, *viz.*, Na^+, K^+, Ca^{2+}, Mg^{2+}, Mn^{2+}, Fe^{2+}, Co^{2+}, Ni^{2+}, Cu^{2+}, Zn^{2+}, Cd^{2+}, Hg^{2+}, Pb^{2+}, and Ag^+ as studied by fluorescence, absorption, and ESI MS. **L** acts as a sensor for Hg^{2+} by switch-off fluorescence and exhibits a lowest detectable concentration of 1.87 ± 0.1 ppm. The complex formed between **L** and Hg^{2+} is found to be 1:1 on the basis of absorption and fluorescence titrations and was confirmed by ESI MS. The coordination features of the mercury complex of **L** were derived on the basis of DFT computations and found that the Hg^{2+} is bound through an N_2O_2 extending from both the arms to result in a distorted octahedral geometry with two vacant sites. The nanostructural features such as shape and size obtained using AFM and TEM distinguishes **L** from its Hg^{2+} complex and were different from those of the simple mercuric perchlorate. **L** is also suited to sense pyrimidine bases by fluorescence quenching with a minimum detection limit of 1.15 ± 0.1 ppm in the case of cytosine. The nature of interaction of pyrimidine bases with **L** has been further studied by DFT computational calculations and found to have interactions through a hydrogen bonding and NH-π interaction between the host and the guest.

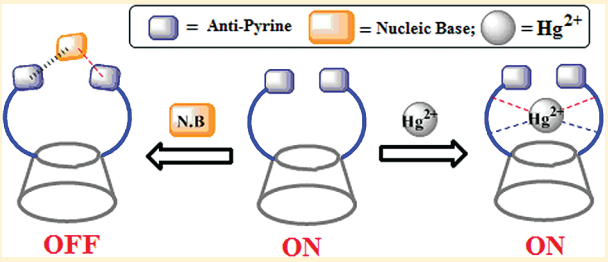

INTRODUCTION

Development of selective chemosensors for the determination of transition and heavy metal ions is an important area of research, because metal ions such as Pb^{2+}, Cd^{2+}, and Hg^{2+} have lethal effects on living systems in addition to their effect in the environmental pollution.[1] Supramolecular systems like calixarenes[2] functionalized with suitable binding cores can act as good hosts for the recognition of ionic and molecular species,[3] though such systems are limited in the literature in case of Hg^{2+} recognition.[4] Calix[4]arenes functionalized with aryl-azo,[5] benzothiazole-azo,[6] benzimidazole,[7] and fluorescent probes such as pyrene, rhodamine,[8] and dansyl fluorophoric groups[9] have been used as ion receptors in the literature. Therefore, the development of molecular receptors that can selectively recognize Hg^{2+} is an important area of research. Recognition of nucleic bases is important in DNA detection, as biosensors and chips are being widely used in biological sciences for the same.[10] A gold electrode based sensor array for selective recognition of purines and pyrimidines has been reported.[11] Ruthenium and osmium complexes of bipyridyl ligands have been used for electrochemical and/or luminescent labeling of biomolecules and hence are sensitive in the recognition of the nucleic acids.[12] Silver nanoparticles capped with a conjugate of calix[4]arene have been reported to discriminate purines from those of pyrimidines.[13] A calix[6]arene-acid derivative is shown to be effectively extracting adenine by forming a complex.[14] Therefore, herein we report the development of a lower rim 1,3-di{4-antipyrine}amide derivative of calix[4]arene (**L**), wherein the antipyrine unit is connected through an amide link for the purpose of selectively recognizing Hg^{2+} in methanol. The **L** also shows selectivity toward pyrimidine bases by fluorescence quenching.

RESULTS AND DISCUSSIONS

Synthesis of the Receptor Molecule (L). The receptor molecule, **L**, was synthesized *via* four known steps[15] starting from *p-tert*-butyl calix[4]arene as shown in scheme 1. The calix[4]arene acid chloride derivative $\mathbf{L_4}$ was made by reacting the diacid derivative, $\mathbf{L_3}$, with $SOCl_2$, followed by coupling with 4-aminoantipyrine to result in **L**. All these molecules including **L** were characterized satisfactorily by ^1H and ^{13}C NMR, ESI MS, HRMS, FTIR, and elemental analysis (Supporting Information 01, 02). The cone conformation of **L** has been revealed by ^1H NMR spectroscopy and was further confirmed by establishing the structure using single crystal XRD.

Crystal Structure of L. Colorless, diffraction quality single crystals of **L** were grown from its EtOH/$CHCl_3$ (1:4) solution. It crystallizes as monoclinic with space group $P2_1/c$. The corresponding details of the structure determination and refinement data are given in Table 1. The crystal structure of **L** given in Figure 1a confirms cone conformation of the conjugate that

Received: October 31, 2011
Published: January 4, 2012

   dx.doi.org/10.1021/jo2022372 | J. Org. Chem. 2012, 77, 1406–1413

Scheme 1. Synthesis of L[a]

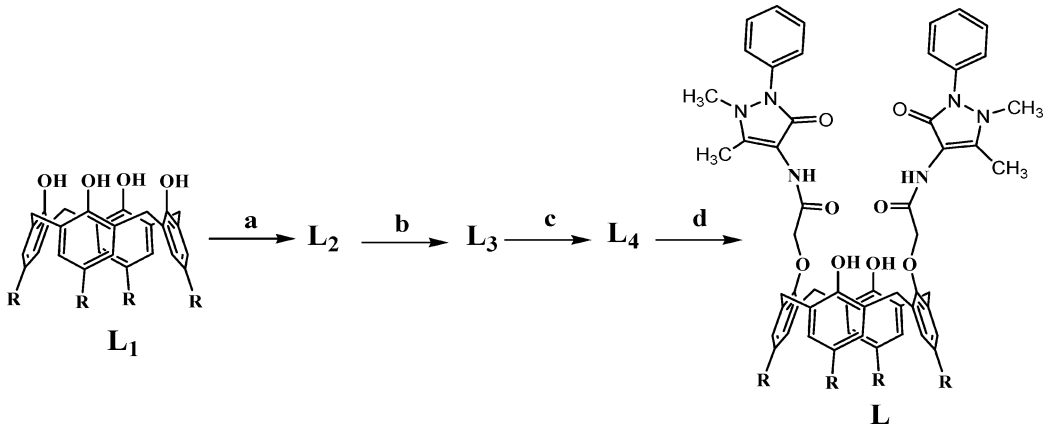

[a](a) Bromoethylacetate/K_2CO_3/acetone; (b) NaOH/C_2H_5OH, reflux; (c) $SOCl_2$/benzene, reflux; (d) 4-aminoantipyrine/Et_3N/THF. R = *tert*-butyl.

Table 1. Crystal Data and Structure Determination Data for L

parameter	value for **L**
empirical formula	$C_{70}H_{82}N_6O_8$, C_2H_6O, H_2O
formula weight	1199.51
wavelength (Å)	0.71073
T/K	120
crystal system	monoclinic
space group	$P2_1/c$ (No. 14)
a (Å)	22.45(7)
b (Å)	11.99(3)
c (Å)	25.56(8)
α (deg)	90
β (deg)	107.797(4)
γ (deg)	90
V (Å^3)	6554.7(4)
Z	4
absorption coefficient (mm^{-1})	0.081
F(000)	2576
D_{calcd} (g/cm^3)	1.215
total reflections	55285
unique reflections	11527
R_{int}	0.051
no. of parameters refined	857
final R ($I > 2\sigma$)	0.0460
wR_2 ($I > 2\sigma$)	0.0855

was also predicted on the basis of NMR studies in solution. The metric data for **L** is given in Supporting Information 03. The circular hydrogen bonding observed between the donor···acceptor pairs at the calix[4]arene lower rim are 2.7619(19) and 2.7790(19) Å with the corresponding angles of 170(2)° and 171(2)°, respectively. **L** has been crystallized with a molecule each of ethanol and water. Ethanol was found to be trapped inside the aromatic cavity of calix[4]arene while the water is present in the lattice. There exists hydrogen bonding between the −C═O of antipyrine and O−H of water with an O···O distance of 2.848(2) Å and hydrogen bond angle of 172(3)° (Figure 2). One of the arms is bent by forming an intra-rim N−H···O hydrogen bond with an N···O distance of 3.10 Å. The amide CO of the bent arm points outside the

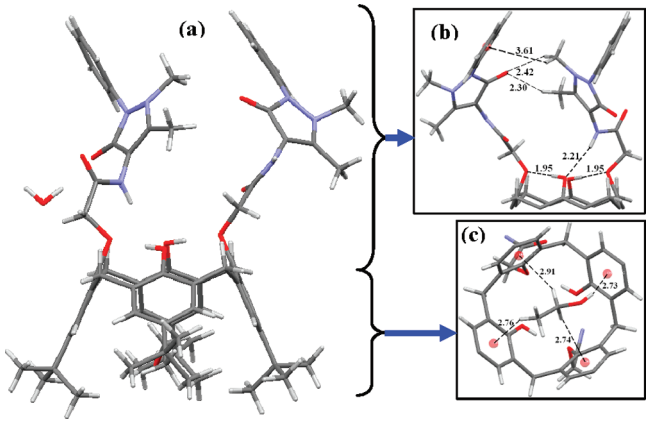

Figure 1. (a) X-ray crystal structure of the receptor molecule, **L**·EtOH.H_2O. (b) Intramolecular C−H···π interactions observed between the arms. (c) C−H···π interactions observed between ethanol and the calix[4]arene cavity.

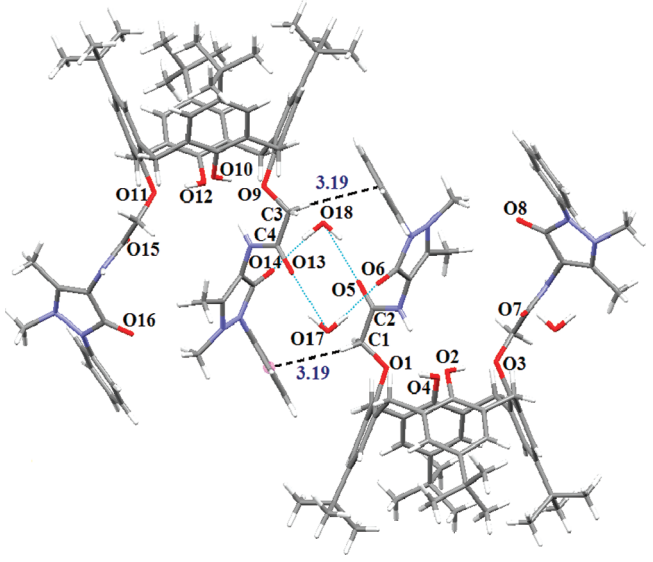

Figure 2. Dimer formed from two receptor (**L**) molecules *via* lattice water and C−H···π interactions in the crystal lattice.

dx.doi.org/10.1021/jo2022372 | J. Org. Chem. 2012, 77, 1406−1413

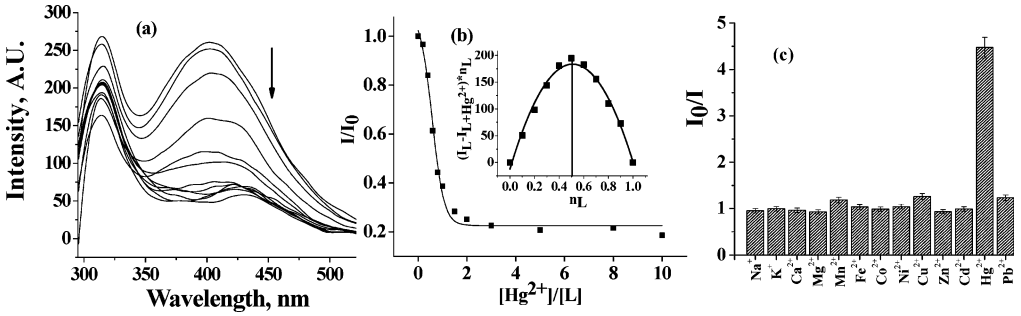

Figure 3. Fluorescence titration of **L** with metal ions. (a) Spectral traces of **L** as a function of added Hg^{2+} to result in $[Hg^{2+}]/[L]$ mole ratio from 0 to 10.0 in methanol. (b) Relative fluorescence intensity (I/I_0) versus $[Hg^{2+}]/[L]$ mole ratio at 400 nm. Inset: Job's plot obtained from fluorescence data, where I_L is fluorescence intensity of receptor **L** and $I_{L+Hg}{}^{2+}$ is fluorescence intensity of the mercury ion complex. n_L is mole fraction of **L**. (c) Histogram of highest I_0/I ratio indicating the quenching fold for the titration of **L** by different metal ions. Error bars were given on the basis of three different measurements.

calix[4]arene cavity while the other amide CO points toward the calix[4]arene core. The centroid to centroid distance of the aryl moieties of the antipyrine lies at a distance of 6.87 Å with a tilt angle of 9.5° and hence cannot exhibit any intramolecular $\pi\cdots\pi$ interaction in **L** (Figure 1b). However the crystal packing structure shows (Figure 1c) intermolecular C1−H$\cdots\pi$ interaction with the centroid of the ring at a distance of 3.19 Å. In the lattice, the two neighboring **L** are connected through two water molecules (O18 and O17) by exhibiting hydrogen bonds with the amide CO at a distance of 2.84 and 2.93 Å and hydrogen bond angles of 147° and 172°, respectively. The ethanol molecule that is trapped in the calix[4]arene cavity exhibits CH$\cdots\pi$ interaction with all of the four aromatic moieties, with CH$\cdots\pi$ distances of 2.73 − 2.91 Å from the center of the aromatic ring (Figure 1c).

As the arms of **L** possesses groups that are well suited for the interaction with the incoming guest species, besides exhibiting fluorescence emission, the **L** has been explored for its ion and molecular recognition studies using absorption and fluorescence spectroscopy.

Metal Ion Binding Studies in Methanol. The metal ions, *viz.*, Na^+, K^+, Ca^{2+}, Mg^{2+}, Mn^{2+}, Fe^{2+}, Co^{2+}, Ni^{2+}, Cu^{2+}, Zn^{2+}, Cd^{2+}, Pb^{2+}, and Ag^+ were studied for their binding properties with **L** at 20 μM concentration by carrying out titrations as given in the Experimental Section. The studies were carried out by exciting the solutions at 280 nm and recording the fluorescence spectra in the range of 295−530 nm in methanol. During the titration, the fluorescence intensity of **L** at 400 nm decreases as a function of the concentration of Hg^{2+} added (Figure 3) and attains saturation at ~2 equiv. Thus the titration of **L** with Hg^{2+} results in a stoichiometric reaction. The emission λ_{max} of **L** is shifted to red by 25 nm upon complexation with Hg^{2+}. However, similar titrations carried out with other metal ions, such as Na^+, K^+, Ca^{2+}, Mg^{2+}, Mn^{2+}, Fe^{2+}, Co^{2+}, Ni^{2+}, Cu^{2+}, Zn^{2+}, Cd^{2+}, Pb^{2+}, and Ag^+, exhibited minimal or no change in the fluorescence intensity as can be seen from Figure 3 (Supporting Information 04). The binding constant of **L** with Hg^{2+} was derived based on the Benesi−Hildebrand equation to yield a K_a of 10550 ± 700 M^{-1}. The quantum yields of **L** and its Hg^{2+} complex were found to be 0.010 and 0.004 by using naphthalene as standard. The minimum detection of Hg^{2+} by **L** is found to be (1.87 ± 0.1) ppm (Supporting Information 05) as derived on the basis of fluorescence studies.

UV−vis Absorption Studies. UV−vis absorption titrations were carried out between **L** and Hg^{2+} at a concentration of 63 μM in methanol (see Experimental Section for details), and the study shows a decrease in the absorption intensity at 280 nm and an increase in the absorbance at 315 and 256 nm (Figure 4).

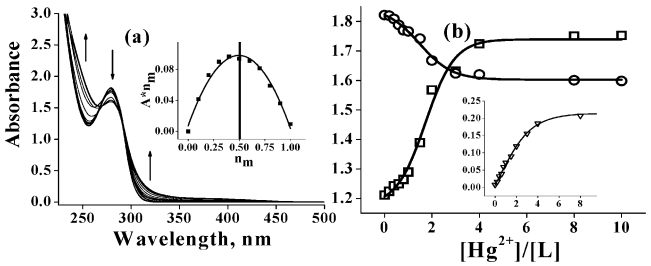

Figure 4. Absorption titration of **L** with Hg^{2+}. (a) Spectral traces observed in the titration of **L** with Hg^{2+} in methanol at varying mole ratio. Inset: Job's plot of n_L versus $A{\cdot}n_m$, where n_m is mole fraction of Hg^{2+} ion and A is absorbance. (b) Plot of absorbance vs mole ratio of $[Hg^{2+}]/[L]$ for different bands (○ = 280, □ = 256 nm and inset ▽ = 315 nm).

An isosbestic point was observed at 294 nm supporting the complex formation. Job's plot obtained using the fluorescence and absorption spectra indicated the formation of a 1:1 complex between Hg^{2+} and **L**. However the absorption titration carried out with all the other metal ions showed no significant change, indicating their noninteractive nature with **L**. Even the ions from the same group, *viz.*, Zn^{2+} and Cd^{2+}, do not bind to **L** (Supporting Information 06)

Electrospray Mass Spectra of L with Hg^{2+}. The complex formed between **L** and Hg^{2+} has been further confirmed to be 1:1 based on ESI MS. The mass spectra yielded a molecular ion peak for 1:1 complex at m/z of 1335.7, where its isotopic peak pattern supports the presence of Hg^{2+} (Figure 5; Supporting Information 07).

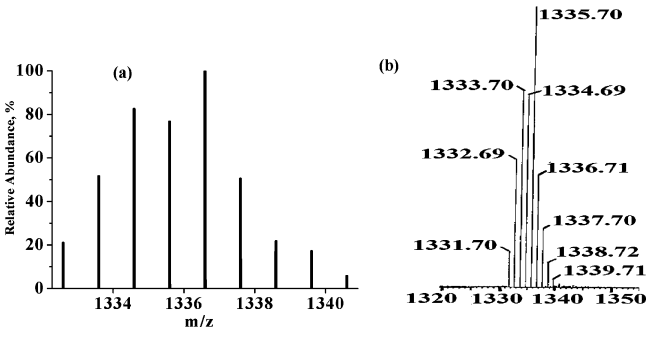

Figure 5. ESI MS spectrum of $[L\text{-}Hg^{2+}]$ complex. (a) Theoretical isotopic pattern for $[L+Hg^{2+}]$ ion. (b) Experimentally observed molecular ion peak.

dx.doi.org/10.1021/jo2022372 | J. Org. Chem. 2012, 77, 1406−1413

Competitive Metal Ion Titration by Fluorescence Spectroscopy. In order to evaluate the efficiency of the receptor **L** in recognizing Hg^{2+} in the presence of other metal ions, competitive titrations were carried out by fluorescence spectroscopy. The spectra were recorded for [**L** + xM^{n+}] against Hg^{2+} in the presence of 30 equiv of biologically relevant metal ions, such as Na^+, K^+, Ca^{2+}, Mg^{2+}, or 5 equiv of Mn^{2+}, Fe^{2+}, Co^{2+}, Ni^{2+}, Cu^{2+}, Zn^{2+}, Cd^{2+}, Pb^{2+}, or Ag^+ ions. The presence of excess equivalents of metal ions did not affect the quenching characteristics and the emission intensity of **L** when titrated with Hg^{2+}. Further, the titrations carried out between [**L** + $2Hg^{2+}$] and M^{n+} did not exhibit any significant change in the fluorescence intensity as can be noted from Figure 6. Thus **L** can recognize Hg^{2+} even in the presence of other metal ions.

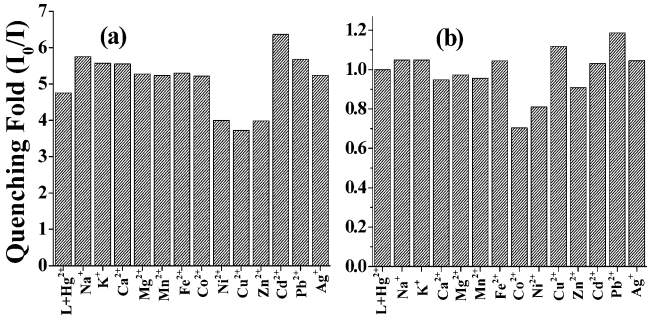

Figure 6. Histograms showing quenching fold. Titration of (a) [**L** + x equiv M^{n+}] against Hg^{2+} and (b) [**L** + 2 equiv Hg^{2+}] against M^{n+}, x = 30 for Na^+, K^+, Ca^{2+}, Mg^{2+} and x = 5 for other metal ions.

Computational Study of the Structural Features of the 1:1 Complex of L with Hg^{2+}. As no single crystals could be obtained for the complex of **L** with Hg^{2+}, its structure could not be established. Therefore, in order to understand the interactions present between **L** and Hg^{2+}, computational studies were carried out in a systematic fashion by starting from semiempirical and then going through HF followed by DFT, in a cascade fashion. As the formation of 1:1 species was already established by Job's plot and ESI MS, the [**L**-Hg^{2+}] complex was modeled using the Gaussian 03 package.[16] Prior to assuming the initial guess model for the computational calculations, structure of **L** was optimized (Figure 7a) taking the coordinates from the crystal structure and chopping off the *tert*-butyl groups to reduce the computational time. The structure was then optimized by using different theories. The Hg^{2+} ion has been placed far away from the predicted binding region. The optimization of the corresponding complex between **L** with Hg^{2+} was started in a cascade fashion by going through AM1 → HF/CEP-121G → B3LYP/CEP-121G. In the optimized complex (Figure 7b), the Hg^{2+} was bonded to the two amide-N atom. The bond length and bond angle around the Hg^{2+} center are N1/N2···Hg = 2.17 Å and N1···Hg···N2 = 165°, respectively. The two amide-O atoms, *viz.*, O1 and O2, also provide additional interactions at a Hg···O distance of 2.562 and 2.768 Å, which is within the sum of vander Waal's radii. Thus, the optimized structure reveals a distorted octahedral geometry around Hg^{2+} with two vacant sites of which one lies in the equatorial plane (Figure 7c) and other lies trans to O2. Such structure around the Hg^{2+} indeed exhibited ~7.6 kcal/mol additional stabilization when compared to a binding model of N−Hg−O2═C_{amide} (Supporting Information 08).

Nanostructural Features of L and Its Mercury Complex by AFM. AFM images of **L** and its Hg^{2+} complex shows that the particles were well spread over the mica sheet. The morphological features of free **L** and this in the presence of Hg^{2+} are quite distinct in their sizes. While **L** alone forms almost uniform particles of size 250 ± 30 nm with good separation, those observed in the presence of Hg^{2+} were shortened substantially to have particles with sizes of 45 ± 5 and 80 ± 10 nm with higher packing density in the latter case. However, both of these particles are close to spherical in shape. Thus, the presence of Hg^{2+} induces the formation of smaller particles as shown in Figures 8 and 9. Therefore, the larger size of the particles observed in case of **L** may be attributable to the aggregation due to the presence of hydrophobic groups, and these become much small in the presence of Hg^{2+} owing to the coordination ability of **L** through amide nitrogen and carbonyl oxygen centers. In effect, the structural features observed in AFM for **L** differs clearly from its complex of Hg^{2+}. The structural features observed for **L** and its mercury complex differs substantially from that observed with the simple salt, *viz.*, mercury perchlorate. The height of the particles of **L** exhibits an average value of 90 ± 10 nm. However, in the presence of Hg^{2+} the height of these particles decrease substantially to result in 12 ± 2 and 4 ± 2 nm for the larger and smaller size ones, respectively.

Nanostructural Features of L and Its Mercury Complex by TEM. The shape and size of the particles of **L**, its Hg^{2+} complex, and simple mercury perchlorate observed in TEM micrographs can be seen from Figure 10. **L** shows spherical particles with two different size distributions, one ~550 nm and the other ~900 nm, and the particles possess a dark core region that is surrounded by a lighter shell (Figure 10a,b,g). However in

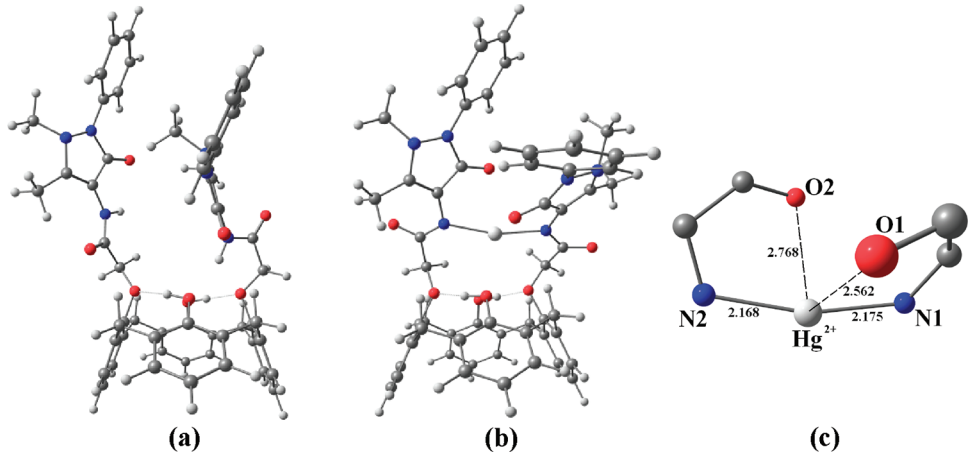

Figure 7. DFT optimized structures: (a) **L**; (b) [**L**-Hg^{2+}] complex; and (c) the binding core around Hg^{2+}. The bond lengths given in panel (c) are in Å.

dx.doi.org/10.1021/jo2022372 | J. Org. Chem. 2012, 77, 1406–1413

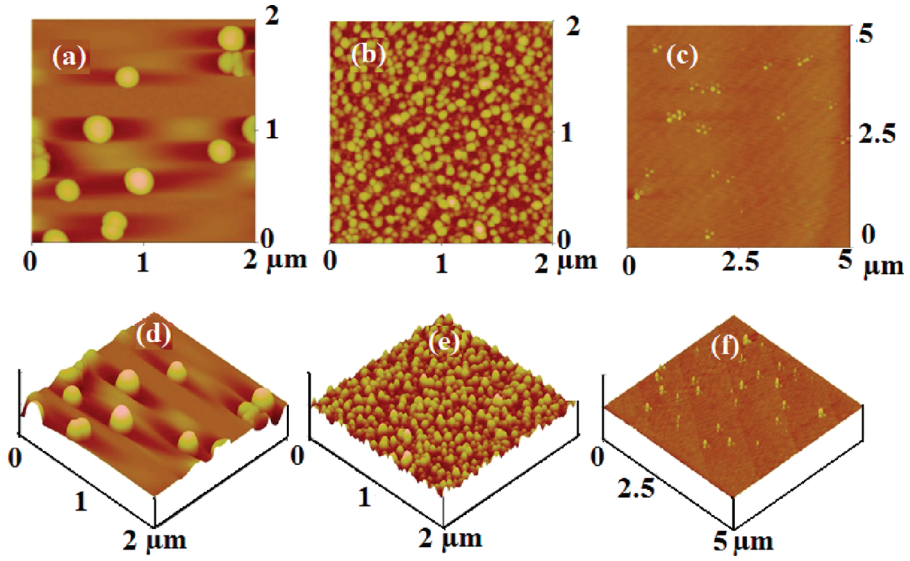

Figure 8. AFM micrographs: (a, d) **L**; (b, c) [**L**-Hg^{2+}] complex; (c, f) $Hg(ClO_4)_2$.

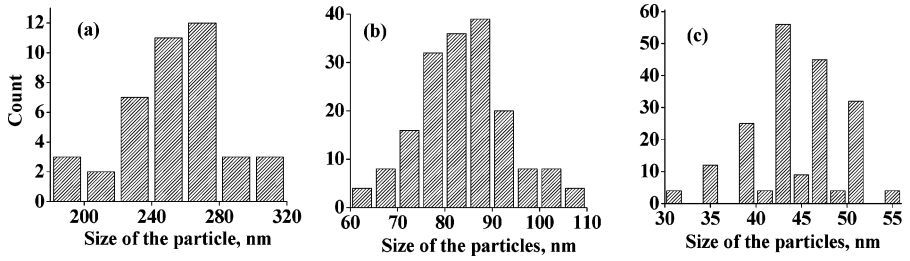

Figure 9. Particle size distribution: (a) **L**, (b) bigger particles of **L** in presence of Hg^{2+}, and (c) smaller particles of **L** in presence of Hg^{2+}.

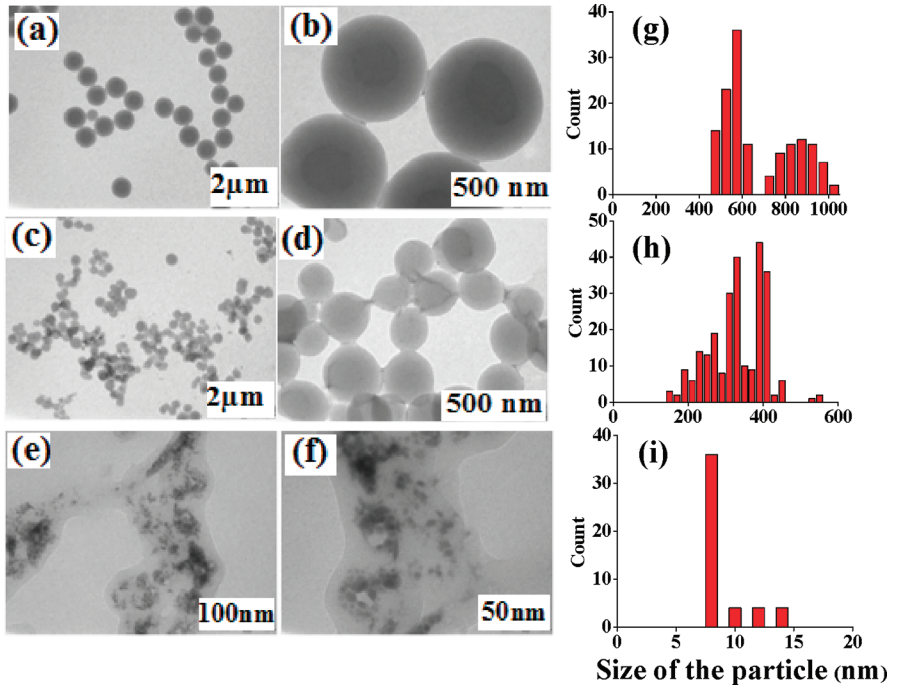

Figure 10. TEM micrographs: (a, b) **L**; (c, d) **L** in the presence of Hg^{2+}; (e, f) simple $Hg(ClO_4)_2$ that is used as control. Size distribution of the particles: (g) **L**; (h) **L** in presence of Hg^{2+}; and (i) simple $Hg(ClO_4)_2$.

the presence of Hg^{2+}, the average size of the particles is reduced and is found in the range of 200−400 nm. In the presence of Hg^{2+}, the particles are deformed from spherical shape, resulting in dumbbell shapes, and are well interconnected. When the particles of **L** come closer in the presence of Hg^{2+} with increased connectivity, the dark core region of **L** disappears. This may result

dx.doi.org/10.1021/jo2022372 | J. Org. Chem. 2012, 77, 1406−1413

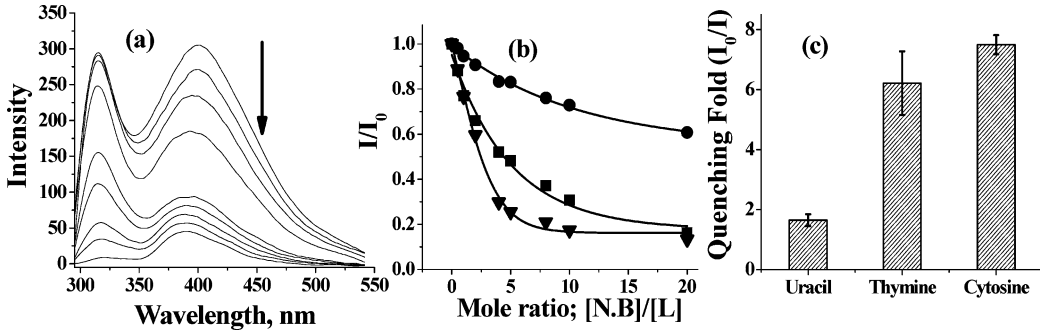

Figure 11. Fluorescence titration of **L** by pyrimidine bases. (a) Spectral traces of **L** as a function of added [cytosine] at varying mole ratios. (b) Relative fluorescence intensity (I/I_0) versus [nucleic base]/[**L**] mole ratio at 400 nm (▼= cytosine, ■ = thymine, and ● = uracil). (c) Histogram of I_0/I ratio indicating highest quenching fold. Error bars were given based on three different measurements.

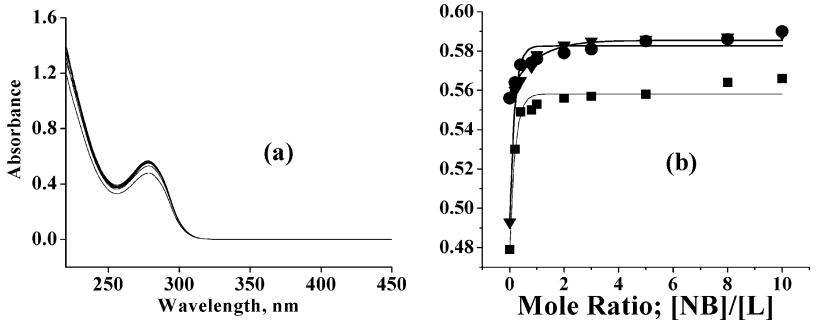

Figure 12. Absorption titration of **L** with pyrimidine bases. (a) Spectral traces of **L** as a function of added [cytosine] at varying mole ratios in methanol. (b) Absorbance versus [nucleic base]/[**L**] mole ratio at 280 nm (■ = cytosine, ● = thymine, and ▼= uracil).

from the coordination of $Hg^{2+}$with **L**. The greater communication among the particles with increased connectivity in the presence of Hg^{2+} may be of further research interest. However, the mercury perchlorate control, under the same conditions, exhibits predominantly mono-dispersed particles of ~8 nm size. Thus the nanostructural features of **L** differ distinctly from those of its Hg^{2+} complex, and the size and shape of both of these differ from those of simple mercury perchlorate

Fluorescence Titrations with Nucleic Bases. The pyrimidine bases cytosine, uracil, and thymine were studied for their recognition by **L**. The studies were carried out by exciting the solutions at 280 nm and recording the fluorescence spectra in the range of 295−530 nm in methanol by taking 20 μM solutions of **L** (Figure 11; Supporting Information 09). Control experiments were carried out simultaneously with the bases alone, and the corresponding data were subtracted from the original spectra. The results showed quenching behavior for all the three nucleic bases, and the extent of quenching follows the order cytosine ≥ thymine ≫ uracil. However, the adenine and guanine could not be studied owing to their strong emission when excited at 280 nm. The minimum detectable concentration based on fluorescence quenching is 1.15 ± 0.1 and 1.41 ± 0.1 ppm for cytosine and thymine, respectively (Supporting Information 10).

Absorption Titrations with Nucleic Bases. Absorption titrations were carried out with **L** at 20 μM with varying equivalents of the nucleic bases cytosine, thymine, and uracil in methanol (Figure 12). Control experiments were also carried out simultaneously with the bases alone, and the corresponding data were subtracted from the original ones. The results exhibited an increase in the absorbance at 280 nm band upon addition of these nucleic bases (Supporting Information 11).

Computational Study of the Structural Features of the Interaction of Nucleic Bases with L. As substantial fluorescence quenching was noticed in the titration of cytosine and thymine with **L**, the nature of the interaction between the nucleic base and **L** were modeled by DFT computational studies as carried out using Gaussian 03 package.[16] Prior to assuming the initial guess model, the nucleic bases were independently optimized. In order to generate the **L**-pyrimidine base complex, the bases were placed far away from the receptor **L**. The optimization of the corresponding complex between **L** with cytosine and thymine were carried out at B3LYP/CEP-121G. In both the cases, the bases were bound to the receptor molecule through a H-bonding and an N−H···π interaction as can be seen from Figure 13 (Supporting Information 12 and 13).

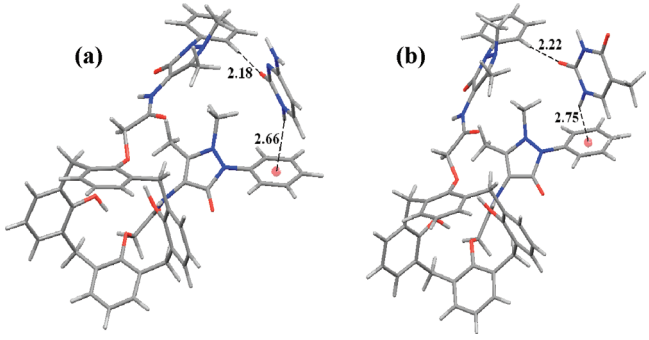

Figure 13. DFT optimized structures: (a) **L**-cytosine complex, and (b) **L**-thymine complex. The distances given in the figure are in Å. The H-bonding angle between O···H−C_{Ar} is 177.1° and 164.3°, respectively.

At B3LYP/CEP-121G level, the stabilization energies computed using the formula $\Delta E_s = E_A - [E_L + E_{NB}]$ {where E_A is

dx.doi.org/10.1021/jo2022372 | J. Org. Chem. 2012, 77, 1406−1413

the total energy of the adduct, E_L is the total energy of the calixarene derivative, and E_{NB} is that of the nucleic base} yielded −14.5 and −8.7 kcal/mol, respectively, for the interaction of cytosine and thymine with **L**.

Conclusions and Correlations. A structurally characterized antipyrine conjugate of 1,3-diamido-calix[4]arene (**L**) exhibits selective recognition of Hg^{2+}. The selectivity has been demonstrated by fluorescence, absorption, and ESI MS spectroscopy. The interaction of Hg^{2+} quenches the fluorescence of **L** observed at 400 nm. **L** is selective and sensitive toward Hg^{2+} over 14 other biologically important metal ions studies, *viz.*, Na^+, K^+, Ca^{2+}, Mg^{2+}, Mn^{2+}, Fe^{2+}, Co^{2+}, Ni^{2+}, Cu^{2+}, Zn^{2+}, Cd^{2+}, Pb^{2+}, and Ag^+. Even the other ions from the same group, Zn^{2+} and Cd^{2+}, do not bind to **L**. None of the M^{n+} ions studied impedes the interaction of Hg^{2+} with **L** as shown by competitive fluorescence titrations. The receptor **L** has been shown to be sensitive with a minimum detection limit of 1.87 ± 0.1 ppm Hg^{2+}. Fluorescence and absorption spectroscopy provides information for the formation of a 1:1 complex between Hg^{2+} and **L**, and ESI MS confirms this fact by exhibiting a peak for [**L**-Hg^{2+}] ion with isotopic pattern for mercury. The Hg^{2+} binding characteristics of **L** has been studied by computational calculations at DFT level, and the optimized structure exhibited a N_2O_2 core with distorted octahedral geometry around Hg^{2+} with two vacant sites of which one lies in the equatorial plane and other lies trans to O2. The nanostructural features observed using AFM and TEM clearly differentiate **L** from its complex with Hg^{2+}. **L** exhibits differential sensitivity toward the pyrimidine bases by exhibiting quenching of fluorescence emission to different extents and thereby provides a means to detect these bases. The fluorescence quenching follows the order cytosine ≥ thymine ≫ uracil. The interaction of pyrmidines with **L** was further studied by computational calculations. The computational results show the nature of interaction of pyrimidnes, *viz.*, cytosine and thymine, as primarily through hydrogen bonding and N−H···π interaction. Thus **L** acts a potential sensor for Hg^{2+} and for pyrimidine nucleic bases.

EXPERIMENTAL SECTION

Synthesis and Characterization Data for the Compounds L_1, L_2, L_3, and L. The derivatives L_1, L_2, and L_3 have been prepared by literature reported procedures.[15] **L** was prepared from diacid chloride derivative, L_3 by following the procedure given below. All the derivatives were characterized satisfactorily using suitable analytical techniques.

Receptor L. To a suspension of 4-aminoantipyrine (1.203 g, 5.92 mmol) and Et_3N (1.50 mL, 10.75 mmol) was added dry THF (60 mL), and the mixture was stirred under an argon atmosphere. Diacid chloride L_4 (2.16 g, 2.70 mmol) in dry THF (60 mL) was added dropwise to this reaction mixture. Immediately, a yellowish precipitate was formed, and stirring was continued for 48 h at room temperature. After filtration, the filtrate was concentrated to dryness. A yellow solid was obtained that was extracted with $CHCl_3$ and washed with water and then with brine, and the organic layer was dried with anhydrous $MgSO_4$. The filtrate was concentrated to dryness and recrystallized from $CHCl_3$/EtOH. Yield 71%. Anal. (% found) C, 74.15; H, 7.35; N, 7.30; (% required) C, 74.05; H, 7.28; N, 7.42. FTIR (KBr matrix, cm^{-1}): 3430 (ν_{OH}); 1694, 1650 ($\nu_{C=O}$). ^1H NMR (400 MHz, $CDCl_3$, δ ppm): 10.22 (s, 2H); 7.69 (s, 2H); 7.36 (s, 10H); 6.98 (s, 4H); 6.81 (s, 4H), 4.69 (s, 4H); 4.24 (d, 4H, J = 13.2 Hz); 3.30 (d, 4H, J = 13.4 Hz); 3.06 (s, 6H) 2.20 (s, 6H) 1.18 (s, 18H), 0.943 (s, 18H). ^{13}C NMR: ($CDCl_3$, δ ppm): 12.3, 31.0, 31.7, 32.4, 33.9, 34.1, 36.5, 75.4, 109.3, 123.6, 125.4, 126.1, 127.6, 129.0, 132.6, 135.0, 142.5, 147.7, 149.4, 149.9, 150.2, 161.2, 168.2, 124.2, 124.8, 127.3, 129.6, 130.1, 134.2, 151.8, 156.2, 168.1. ESI MS: *m/z* (intensity %, fragment) 1135.83 (100, $[M + H]^+$). HRMS (EI): calcd for $C_{70}H_{83}N_6O_8$ $[M + H]^+$ *m/z* 1135.6272, found *m/z* 1135.6227.

Crystal Structure Determination by Single Crystal XRD. Single crystals suitable for X-ray diffraction were obtained for **L**, and the crystal data are given in Table 1. Single crystal X-ray diffraction data were collected on an OXFORD DIFFRACTION XCALIBUR-S CCD system with graphite−monochromated Mo Kα radiation by ω-2θ scan mode and the absorption corrections were applied by using multiscan method. The structure determinations were done by direct methods, and the refinement of the atomic parameters based on full-matrix least-squares on F^2 were performed using the SHELX-97 programs. All hydrogen atoms were geometrically fixed and allowed to refine using a riding model, wherever the difference Fourier did not result in the position of hydrogen. Most of the O-bound hydrogen positions were recovered from the difference Fourier maps and were refined isotropically. All non-hydrogen atoms were refined anisotropically.

Fluorescence Titrations. All fluorescence titrations were carried out on a fluorescence spectrometer at 280 nm excitation wavelength in a 1 cm quartz cell. Bulk solutions (12×10^{-4} M) of **L** were freshly made before each set of experiments by dissolving **L** in $CHCl_3$ (50 μL) and then making up the desired concentration with methanol. The metal perchlorate salts were made at 12×10^{-4} M in methanol. The fluorescence titrations were carried out by exciting the solution at 280 nm after adding the appropriate volume of metal salt solution to result in the requisite mole ratios of $[M^{n+}]/[L]$, yet maintaining the final [**L**] as 20 μM in a total solution volume of 3 mL achieved by diluting with solvent.

Absorption Titrations. Bulk solutions were prepared by similar procedure as in fluorescence studies, but **L** and metal perchlorate salts were made at 5×10^{-3} M concentration. Titrations were performed by varying equivalents of M^{n+} from 0.2 to 10 and fixing the concentration of **L** at 63 μM.

AFM Studies. Solutions of **L** and Hg^{2+} were prepared at 6×10^{-5} M concentration in methanol. The receptor **L** was initially dissolved in 100 μL of $CHCl_3$ and then made up with methanol to the desired concentration. The stock solutions of **L**, **L**-Hg^{2+}, and Hg^{2+} were sonicated for 10 min, after which a 50−70 μL aliquot was taken and spread over a mica sheet using the drop cast method. The samples were then dried and analyzed by AFM technique.

TEM Studies. Solutions of **L** and Hg^{2+} were prepared at 3×10^{-2} M concentration in methanol. The receptor **L** was initially dissolved in 100 μL of $CHCl_3$ and then in methanol. The stock solutions of **L**, **L**-Hg^{2+}, and Hg^{2+} were sonicated for 10 min, after which a 50−70 μL aliquot was taken and spread over a carbon-coated grid using the drop cast method.

ASSOCIATED CONTENT

Supporting Information

^1H, ^{13}C NMR spectra of **L**, ESI-MS and HRMS data for **L**, crystal structure details of **L**, fluorescence titrations spectra with different metal ions, minimum detection limit of Hg^{2+} by **L**, absorption titration spectra of **L** with Zn^{2+} and Cd^{2+}, ESI-MS spectrum of [**L**-Hg] complex, computational data, fluorescence titration spectra of **L** with thymine and uracil, minimum detection limit of thymine and cytosine by **L**, absorption titrations with nucleic bases, Cartesian coordinates for DFT optimized [**L**-thymine] complex, and Cartesian coordinates for DFT optimized [**L**-cytosine] complex. This material is available free of charge via the Internet at http://pubs.acs.org.

AUTHOR INFORMATION

Corresponding Author

*Tel: +91-22-25767162. Fax: +91-22-25723480. E-mail: cprao@iitb.ac.in.

■ ACKNOWLEDGMENTS

C.P.R. acknowledges financial support from DST, CSIR, and DAE BRNS. A.M. acknowledges CSIR, and K.T. acknowledges UGC for their fellowships. J.D. acknowledges DRDL for allowing registration for the Ph.D. program at IIT Bombay. We also acknowledge FIST (Physics)-IRCC central SPM facility of IIT Bombay for AFM studies and CRNTS(SAIF) of IIT Bombay for TEM facility. We thank Dr. Roymon Joseph for some experimental help.

■ REFERENCES

(1) (a) Yantasee, W.; Warner, C. L.; Sangvanich, T.; Addleman, R. S.; Carter, T. G.; Wiacek, R. J.; Fryxell, G. E.; Timchalk, C.; Warner, M. G. *Environ. Sci. Technol.* **2007**, *41*, 5114. (b) Boening, D. W. *Chemosphere* **2000**, *40*, 1335. (c) Kim, H. N.; Lee, M. H.; Kim, H. J.; Kim, J. S.; Yoon, J. *Chem. Soc. Rev.* **2008**, 1465. (d) Nolan, E. M.; Lippard, S. J. *Chem. Rev.* **2008**, *108*, 3443. (e) Cheng, T.; Xu, Y.; Zhang, S.; Zhu, W.; Qian, X.; Duan, L. *J. Am. Chem. Soc.* **2008**, *130*, 16160.

(2) (a) Rao, C. P.; Dey, M. *Encycl. Nanosci. Nanotechnol.* **2004**, *1*, 475. (b) Gutsche, C. D. *Calixarenes*; Royal Society of Chemistry: Cambridge, U.K., 1989.

(3) (a) Higuchi, Y.; Narita, M.; Niimi, T.; Ogawa, N.; Hamada, F.; Kumagai, H.; Iki, N.; Miyano, S.; Kabuto, C. *Tetrahedron* **2000**, *56*, 4659. (b) Narita, M.; Higuchi, Y.; Hamada, F.; Kumagai, H. *Tetrahedron Lett.* **1998**, *39*, 8687. (c) Park, S. Y.; Yoon, J. H.; Hong, C. S.; Souane, R.; Kim, J. S.; Matthews, S. E.; Vicens, J. *J. Org. Chem.* **2008**, *73*, 8212. (d) Metivier, R.; Leray, I.; Valeur, B. *Chem. Commun.* **2003**, 996. (e) Buie, N. M.; Talanov, V. S.; Butcher, R. J.; Talanova, G. G. *Inorg. Chem.* **2008**, *47*, 3549. (f) Ju, H.; Lee, M. H.; Kim, J.; Kim, J. S.; Kim, J. *Talanta* **2011**, *83*, 1359. (g) Liu, C.-W.; Huang, C.-C.; Chang, H.-T. *Anal. Chem.* **2009**, *81*, 2383.

(4) (a) Rao, C. P.; Joseph, R. *Chem. Rev.* **2011**, *111*, 4658. (b) Leray, I.; Valeur, B. *Eur. J. Inorg. Chem.* **2009**, 3525. (c) Yanfei, Y.; Xiaodan, C.; Malgorzata, S.; Richard, A.; Bartsch, A. *Tetrahedron* **2010**, *66*, 447.

(5) (a) Kao, T.-L.; Wang, C.-C.; Pan, Y.-T.; Shiao, Y.-J.; Yen, J.-Y.; Shu, C.-M.; Lee, G.-H.; Peng, S.-M.; Chung, W.-S. *J. Org. Chem.* **2005**, *70*, 2912. (b) Ho, I.-T.; Lee, G.-H.; Chung, W.-S. *J. Org. Chem.* **2007**, *72*, 2434.

(6) Bingol, H.; Kocabas, E.; Zor, E.; Coskun, A. *Talanta* **2010**, *82*, 1538.

(7) Joseph, R.; Ramanujam, B.; Acharya, A.; Khutia, A.; Rao, C. P. *J. Org. Chem.* **2008**, *73*, 5745.

(8) Lee, Y. H.; Lee, M. H.; Zhang, J. F.; Kim, J. S. *J. Org. Chem.* **2010**, *75*, 7159.

(9) Pandey, S.; Azam, A.; Pandey, S.; Chawla, H. M. *Org. Biomol. Chem.* **2009**, *7*, 269.

(10) Tsuzuki, S.; Kawanishi, Y.; Abe, S. *Biosens. Bioelectron.* **2005**, *20*, 1452.

(11) Hirsch, T.; Kettenberger, H.; Wolfbeis, O. S.; Mirsky, V. M. *Chem. Commun.* **2003**, 432.

(12) Vrabel, M.; Horakova, P.; Pivonkova, H.; Kalachova, L.; Cernocka, H.; Cahova, H.; Pohl, R.; Sebest, P.; Havran, L.; Hocek, M.; Fojta, M. *Chem.—Eur. J.* **2009**, *15*, 1144.

(13) Tauran, Y.; Grosso, M.; Brioude, A.; Kassab, R.; Coleman, A. W. *Chem. Commun.* **2011**, *47*, 10013.

(14) Shimojo, K.; Oshima, T.; Goto, M. *Anal. Chim. Acta* **2004**, *521*, 163.

(15) Collins, E. M.; McKervey, M. A.; Madigan, E.; Moran, M. B.; Owens, M.; Ferguson, G.; Harris, S. J. *J. Chem. Soc., Perkin Trans. 1* **1991**, 3137.

(16) Frisch, M. J.; Trucks, G. W.; Schlegel, H. B.; Scuseria, G. E.; Robb, M. A.; Cheeseman, J. R.; Montgomery, J. A., Jr.; Vreven, T.; Kudin, K. N.; Burant, J. C.; Millam, J. M.; Iyengar, S. S.; Tomasi, J.; Barone, V.; Mennucci, B.; Cossi, M.; Scalmani, G.; Rega, N.; Petersson, G. A.; Nakatsuji, H.; Hada, M.; Ehara, M.; Toyota, K.; Fukuda, R.; Hasegawa, J.; Ishida, M.; Nakajima, T.; Honda, Y.; Kitao, O.; Nakai, H.; Klene, M.; Li, X.; Knox, J. E.; Hratchian, H. P.; Cross, J. B.; Adamo, C.; Jaramillo, J.; Gomperts, R.; Stratmann, R. E.; Yazyev, O.; Austin, A. J.; Cammi, R.; Pomelli, C.; Ochterski, J. W.; Ayala, P. Y.; Morokuma, K.; Voth, G. A.; Salvador, P.; Dannenberg, J. J.; Zakrzewski, V. G.; Dapprich, S.; Daniels, A. D.; Strain, M. C.; Farkas, O.; Malick, D. K.; Rabuck, A. D.; Raghavachari, K.; Foresman, J. B.; Ortiz, J. V.; Cui, Q.; Baboul, A. G.; Clifford, S.; Cioslowski, J.; Stefanov, B. B.; Liu, G.; Liashenko, A.; Piskorz, P.; Komaromi, I.; Martin, R. L.; Fox, D. J.; Keith, T.; Al-Laham, M. A.; Peng, C. Y.; Nanayakkara, A.; Challacombe, M.; Gill, P. M. W.; Johnson, B.; Chen, W.; Wong, M. W.; Gonzalez, C.; Pople, J. A. *Gaussian 03*, revision C.02; Gaussian, Inc.: Wallingford, CT, 2004.